Eur Biophys J (2010) 39:1177–1192
DOI 10.1007/s00249-009-0570-6

ORIGINAL PAPER

Highly polar environments catalyze the unfolding of PrP^C helix 1

Martin Lingenheil · Robert Denschlag · Paul Tavan

Received: 5 July 2009 / Revised: 21 October 2009 / Accepted: 14 December 2009 / Published online: 5 January 2010

Abstract The first α-helix (H1) likely plays an important role in the conversion of the cellular prion protein (PrP^C) into its pathogenic isoform (PrP^{Sc}). In this conversion, H1 may either have to unfold or may represent a site of intermolecular contact. A recent molecular dynamics simulation suggested that H1 can unfold if it is detached from the protein core (Hirschberger et al. in Biophys J 90:3908, 2006). It has been hypothesized that the high dielectric constant ε_S of the bulk water environment facilitates the unfolding of H1. To check this hypothesis, we performed a number of replica exchange molecular dynamics simulations of an H1 peptide in solvents of different ε_S. We found that the equilibrium helix fraction in water is less than 40%, in agreement with previous experimental findings, and that the helix unfolds much faster in water than in less polar solvents. The kinetically stabilizing effect of the organic solvents is largely unspecific and correlates well with their dielectric constant ε_S.

Keywords Molecular dynamics · Peptide studies · Secondary structure · Prion protein · Helix 1 · Dielectric constant

Electronic Supplementary Material Supplementary material is available for this article at 10.1007/s00249-009-0570-6 and is accessible for authorized users.

M. Lingenheil · R. Denschlag · P. Tavan (✉)
Department für Physik, LMU München,
Oettingenstraße 67, 80538 Munich, Germany
e-mail: tavan@physik.uni-muenchen.de

Introduction

Transmissible spongiform encephalopathies (TSEs) or prion diseases, such as Creutzfeldt-Jakob disease, Gerstmann-Sträussler-Scheinker syndrome, and fatal familial insomnia in humans, or bovine spongiform encephalopathy, scrapie, and chronic wasting disease in animals, are characterized by a refolding of the cellular prion protein PrP^C into the pathological isoform PrP^{Sc} (Prusiner 1998). In contrast to other known mammalian protein aggregation diseases like Alzheimer's and Parkinson's diseases, TSEs are infectious. According to the protein-only hypothesis (Griffith 1967; Prusiner 1982), this infectivity is due to the (auto)catalytic replication of PrP^{Sc} by a template-guided misfolding of PrP^C (Jarrett and Lansbury Jr 1993; Cohen et al 1994; Eigen 1996).

The overall three-dimensional structure of the monomeric PrP^C is conserved among mammalian species (Wüthrich and Riek 2001). The protein consists of a largely unstructured N-terminal region, which, in humans, extends to about residue 124, and of a globular C-terminal domain, which is composed of two short β-strands, S1 (residues 128–131) and S2 (residues 161–164), forming an antiparallel β-sheet, and of three α-helices, H1 (residues 144–154), H2 (residues 173–194) and H3 (residues 200–228), with H2 and H3 connected by a disulfide-bond between residues 179 and 214 (Zahn et al. 2000). In contrast to the cellular isoform PrP^C, the infectious isoform PrP^{Sc} has hitherto proven unavailable to high-resolution methods of protein structure determination because of its propensity to form fibrillar aggregates (Wille and Prusiner 1999). Yet, as determined by Fourier-transform infrared (FTIR) and by circular dicroism (CD) spectroscopy, the transition from PrP^C to PrP^{Sc} is marked by a distinct increase in β-structure and a moderate loss of α-helix content (Pan et al. 1993; Caughey et al. 1991). These

findings imply that part of the structural changes must comprise also the globular domain, including at least a partial unfolding of H1, H2 or H3.

A recent structure model by Cobb et al. (2007) of in vitro generated PrP amyloid, which is based on data obtained by electron paramagnetic resonance spectroscopy and site-directed spin labeling as well as by hydrogen/deuterium exchange experiments (Lu et al 2007), ascribes the refolding to H2 and H3. The spiral model (DeMarco and Daggett 2004) for PrP^{Sc} protofibrils, which is derived from an altered PrP conformation observed in a molecular dynamics (MD) simulation, excludes the region comprising the three helices completely from major rearrangements and localizes the structural differences between PrP^{C} and PrP^{Sc} in the N-terminal part of the globular domain, while yet another class of so-called β-helix models (Govaerts et al. 2004; Stork et al. 2005; Langedijk et al. 2006) agrees with the spiral model in that H2 and H3 are largely conserved but, in contrast to the spiral model, require that H1 unfolds during the conversion. Indeed, antibody studies suggest that the H1 region becomes either buried or refolded upon formation of PrP^{Sc} (Williamson et al. 1998; Pan et al. 2005). Subsequent studies with antibodies (see, e.g., Pankiewicz et al. 2006 and references therein) as well as several other lines of evidence (Norstrom and Mastrianni 2006; Watzlawik et al. 2006; Solforosi et al. 2007; Yu et al 2007; Hesp et al. 2007) suggest that the H1 region is important for the specific binding of PrP^{C} or a partially unfolded intermediate to the replicative PrP^{Sc} complex.

There is strong evidence that partially unfolded intermediates feature in the conversion of PrP^{C} to PrP^{Sc} (for a review, see Surewicz et al. 2006). In particular, it has been hypothesized that the initial step in the conversion of PrP^{C} is characterized by the detachment of a subdomain (S1–H1–S2) comprising the two β-strands, S1 and S2, and the first α-helix H1 from the relatively stable core (H2–H3) of the globular domain of the protein (Calzolai and Zahn 2003; Schwarzinger et al. 2006; Hirschberger et al 2006; Eghiaian et al. 2007; De Simone et al. 2007). In fact, large-scale rigid body motions and loss of tertiary contacts for the H1 region have been observed in a variety of equilibrium (Gsponer et al 2001; De Simone et al. 2007) and non-equilibrium (Alonso et al. 2002; Levy and Becker 2002; Colacino et al. 2006; Pappalardo et al. 2007) molecular dynamics (MD) simulations. In particular, in a recent MD simulation (Hirschberger et al. 2006) of PrP^{C} carrying the M205R mutation, which disturbs the hydrophobic packing of H1 to the H2–H3 core of the globular domain, H1 detached from the H2–H3 scaffold and subsequently unfolded quickly. This observation led Hirschberger et al. (2006) to the question whether the two events are connected, i.e., whether the packing of the S1–H1–S2 domain to the hydrophobic core of the protein stabilizes H1.

Indeed, the α-helical stability of H1 seems to be context-dependent (Fernández et al. 2008): In pure water, nuclear magnetic resonance (NMR) spectroscopy of short peptides covering the H1 sequence indicates a significant helical propensity for the H1 residues (Sharman et al. 1998; Liu et al. 1999; Jamin et al. 2002; Ziegler et al. 2003). However, a well-formed α-helical conformation that is stable on the NMR time scale would imply that typical patterns of medium-range nuclear Overhauser effects (NOEs) were observed. If mentioned at all, these NOEs were either absent (Sharman et al. 1998; Ziegler et al. 2003) or rare and weak (Liu et al 1999) in the cited studies. Taken together with CD and FTIR spectroscopy data, which indicate a helical content of less than 25% for various H1 peptides (Sharman et al. 1998; Liu et al. 1999; Thompson et al. 2000; Jamin et al. 2002; Tahiri-Alaoui et al. 2003; Ziegler et al. 2003), this suggests that, in aqueous solution, an α-helical conformation exists in rapid equilibrium with essentially isoenergetic random coil conformations. Interestingly, for yet another H1 peptide in water, Kozin et al. (2001) found no α-helical structure at all, but determined a well-defined β-hairpin motif using CD and NMR spectroscopy.

Megy et al. (2004) found that, upon addition of 2,2,2-trifluoroethanol (TFE) as a cosolvent, the β-hairpin peptide studied earlier by Kozin et al. (2001) could be refolded into a well-defined α-helical conformation essentially identical to that of the corresponding sequence portion in PrP^{C}. Similarly, significant concentrations of TFE and other organic cosolvents were shown to stabilize the nascent α-helical conformations of the other H1 peptides (Sharman et al. 1998; Liu et al 1999; Thompson et al. 2000; Tahiri-Alaoui et al. 2003; Ziegler et al. 2003), which are largely unstructured in water. Remarkably, the effect of methanol (MeOH) as a cosolvent is comparable to that of TFE, which is well-known for its specific helix-stabilizing effect (Nelson and Kallenbach 1986). In view of all these data, Hirschberger et al. (2006) hypothesized that the stabilization of H1 as an α-helix by organic cosolvents is largely unspecific and probably due to the lower dielectric constant ε_S of organic solvents. This view nicely agrees with earlier arguments of Morrissey and Shakhnovich (1999), who argued that electrostatic interactions are probably pivotal for the stability of the helical conformation of H1 due to the peptide's unusual abundance of charged residues. Since the dielectric screening of these charges weakens with decreasing ε_S, the peptide-internal electrostatic interactions will become dominant in low-ε_S environments and so does an electrostatically stabilized α-helical conformation. If the stability of H1 should actually be dominated by electrostatic interactions, the detachment of H1 from the H2–H3 scaffold could indeed trigger its subsequent unfolding because the effective ε_S on the surface of the protein's hydrophobic core is smaller than in the bulk solvent.

To check the hypothesis that the stability of the helical conformation of H1 against unfolding mainly depends on the solvent polarity, we performed MD simulations of a 13-residue polypeptide (huH1) covering the sequence portion 144–156 of the human prion protein (huPrP). Here, we used explicit solvent environments with experimental dielectric constants ε_S ranging from 33 (MeOH) to 78 (water). Previous MD simulations of an H1 peptide in water indicated that the complete unfolding of the helix in water may take more than 90 ns at ambient temperature (Dima and Thirumalai 2004). In particular, the strong interactions of the charged amino acids in huH1 may lead to high energy barriers, which have to be crossed in the process of unfolding. Thus, to increase the number of conformational transitions, we applied replica exchange with solute tempering (Liu et al. 2005) (REST), a method that has previously been shown to enhance the convergence of helix folding/unfolding equilibria (Huang et al. 2007; Reichold 2009). However, even with REST it is notoriously difficult to acquire convergence of the folding/unfolding equilibrium (Denschlag et al. 2008). Therefore, as a convergence test and in contrast to previous MD simulations of H1 peptides in water (Dima and Thirumalai 2004; Ji et al. 2005), we start our simulations not only from α-helical, but also from unfolded states.

Methods

Model peptide

The peptide huH1 serving as a model for H1 in our simulations has the sequence Ac-DYEDRYYRENMHR-NH_2, which is equivalent to the sequence 144–156 of huPrP. The N-terminus is capped with an acetyl group (Ac) and the C-terminus with an amino group (NH_2) to exclude electrostatic interactions of the termini with charged side chains because such interactions are absent when H1 is integrated into the protein. In the NMR structure of $huPrP^C$ determined at an acidic pH (Zahn et al. 2000), H1 is two residues shorter (residues 144–154) than our huH1 peptide. We decided to simulate the longer sequence 144–156 identified for H1 in the NMR structure at neutral pH (Calzolai and Zahn 2003) because the positive charge of the C-terminal R156 will, in any case, influence the electrostatics of H1 and, in particular, might contribute to the stability of the helix by favorable interaction with E152 or with the helix dipole (Munoz and Serrano 1994, 1995; Shoemaker et al 1987).

Molecular mechanics force field

In our MD simulations, the peptide was described by the CHARMM22 force field (MacKerell et al. 1998). We applied the CMAP correction (MacKerell et al. 2004) to the potentials of the backbone dihedral angles ϕ and ψ to obtain a better model for the α-helical region of Ramachandran space than with standard CHARMM22. We simulated the huH1 peptide in three different explicit solvent environments: (1) pure water described by the TIP3P (Jorgensen et al. 1983) water model modified as suggested by MacKerell et al. (1998) for usage with the CHARMM22 force field, (2) pure methanol described by the B3 model developed by Walser et al. (2000) and (3) an equimolar mixture of TIP3P water and B3 methanol.

To estimate to what extent the folding/unfolding kinetics of the huH1 peptide can be modified by the viscosity η of the respective solvent, we calculated η for each of the three solvent systems from sample simulations. These simulations were performed at 300 K and covered 2 ns each. All other simulation parameters were identical to those used in the simulations of the solvated peptides described further below. From the trajectories, we calculated the diffusion constants and estimated η using Stokes' law as described by Walser et al. (1999). The resulting estimates are listed in Table 1 and show that the viscosities in the three solvent boxes are quite similar. The values for H_2O and MeOH agree well with published data (Shen and Freed 2002; Walser et al. 2000), which were obtained by different approaches. The viscosity η calculated for the mixed solvent interpolates the values of the pure solvents. Since the differences of the viscosities are small (see Table 1), a major influence on the folding/unfolding kinetics of the solute peptide can be excluded.

MD simulation techniques

All simulations were carried out with the MD simulation program EGO-MMVI (Mathias et al. 2003). The system geometry was given by a rhombic dodecahedron of $R_i = 24$ Å inscription radius and by periodic boundary conditions. We used a multiple time step integration (Eichinger et al. 1997) of Newton's equation of motion with a basic time step of 1 fs. The long-range Coulomb interactions were treated by the combination of structure-adapted multipole expansions (Niedermeier and Tavan 1996) up to quadrupolar order augmented by a moving-

Table 1 Solvent systems: N_S denotes the number of solvent molecules in the system; η denotes the dynamic viscosity; ε_S denotes the dielectric constant assumed for the solvent continuum

Solvent	N_S	η (Pa s)	ε_S
H_2O	2,021	4.9×10^{-4}	78
H_2O/MeOH	1,213	4.7×10^{-4}	55
MeOH	944	4.5×10^{-4}	33

boundary reaction-field approach (Mathias et al 2003). Here, the cutoff radius for the explicit evaluation of the electrostatic interactions was R_i. Beyond this radius, a dielectric continuum was assumed. We chose the dielectric constant ε_S for this continuum using experimental values (Wohlfarth 2008; Mukherjee and Grunwald 1958) for the respective solvent (see column ε_S in Table 1). In the case of the mixture H_2O/MeOH, we assumed that ε_S is the mean of the dielectric constants of the constituents. The van der Waals interactions were calculated explicitly for distances up to 10 Å; at larger distances, a mean-field approach (Allen and Tildesley 1987) was applied. Covalent bonds involving hydrogen atoms were kept fixed using the M-SHAKE algorithm (Kraeutler et al. 2001).

Preparation of the simulation systems

A fully α-helical starting structure of huH1 was generated using the Molden software (Schaftenaar and Noordik 2000) by setting the backbone dihedral angles to the values $\phi_\alpha = -58°$, $\psi_\alpha = -47°$ for an ideal α-helix. This starting structure was placed into the centers of the simulation boxes, which were already filled with the respective solvent models. Any solvent molecule closer than 2 Å to the peptide was deleted. The resulting number N_S of solvent molecules in the respective boxes is given in the second column of Table 1. The generated simulation systems were subjected to an energy minimization followed by three equilibrations of 100 ps duration, in which two Berendsen thermostats (Berendsen et al. 1984) (coupling times 0.1 ps) were separately heating the solvent and the peptide, respectively, to 100, 200 K and finally 300 K. Additionally, a Berendsen barostat (Berendsen et al. 1984) (coupling time 1 ps) equilibrated the system to ambient pressure. For the following production runs, we deactivated the barostat. We also deactivated the peptide thermostat for the production simulations because such a thermostat can interfere with the conformational dynamics of the peptide (Lingenheil et al. 2008).

During the equilibration, the C_α atoms of the peptide were restrained to their initial positions by harmonic potentials with a force constant of 1.0 kcal/(mol/Å^2). When these restraints were removed in the production runs, the initially folded peptides began to unfold. By visual inspection, we identified completely unfolded conformations in these trajectories, which then served as starting structures for the simulations starting from the unfolded state. To refer to a specific simulation, we will use the name of the solvent (cf. Table 1) and the letters "f" for a fully folded (α-helical) start or "u" for a fully unfolded (random coil) start, respectively. Thus, the simulation of the initially fully unfolded huH1 peptide in methanol would be called MeOH/u.

Replica exchange with solute tempering

For each of the prepared simulation systems, 12 copies (replicas) were simulated for 40 ns in parallel at different temperatures (300, 317, 335, 354, 374, 396, 420, 446, 474, 504, 536 and 570 K). In contrast to the more common temperature replica exchange technique, within REST, the potential energies of a given system configuration $\mathbf{x}$ at the temperatures T_i are different and are described by

$$E_i(\mathbf{x}) = E_{\mathrm{pp}}(\mathbf{x}) + \sqrt{\frac{T_i}{T_0}}E_{\mathrm{ps}}(\mathbf{x}) + \frac{T_i}{T_0}E_{\mathrm{ss}}(\mathbf{x}), \quad (1)$$

where $T_0 = 300$ K is the reference temperature, and E_{pp}, E_{ps} and E_{ss} are energies associated with the solute-solute, the solute-solvent and the solvent-solvent interactions, respectively.

According to Eq. (1), only the replica at $T_i = T_0$ has an unchanged potential energy, and, therefore, only this replica is of direct physical relevance. Note that the scaling of the solute-solvent energy E_{ps} with a factor $\sqrt{T_i/T_0}$ in Eq. (1) deviates from the one that Liu et al. (2005) employed in their original implementation of REST. With respect to the electrostatic interactions (including the direct Coulomb interactions and the indirect interactions mediated by the reaction field Mathias et al. 2003), our choice of the scaling factors in Eq. (1) corresponds to a simple scaling of the solvent charges by a factor $\sqrt{T_i/T_0}$, while the form of the energy function (including the dielectric constant of the reaction field continuum) remains unchanged.

We expect that this scaling of the solvent's partial charges as well as the differences in temperature will influence the dielectric response of a given solvent type. On the one hand, the scaling of the potential energy according to Eq. (1) is designed to make the solvent statistics independent of the temperature (Liu et al. 2005). REST thus conserves the orientational statistics of the solvent dipoles for the different temperatures. On the other hand, the strengths of the solvent dipoles increase with the temperature. We therefore expect that, within REST, the solvent's dielectric constant at a temperature T_i is given by $\epsilon_S(T_i) = \sqrt{T_i/T_0}\epsilon_S(T_0)$, implying that the solvent polarity increases with T_i along the temperature ladder. Furthermore, we can conclude that the ratio of the dielectric constants for two different solvent types is the same irrespective of the temperature.

During REST, all pairs of replicas that are simulated at neighboring temperatures T_i and T_j may exchange their temperatures every two picoseconds with a probability

$$P_{ij} = \min\left[1, \exp(-\Delta_{ij})\right] \quad (2)$$

with

$$\Delta_{ij} = \left(\beta_i - \beta_j\right)\left[E_{\mathrm{pp}}(\mathbf{x}_j) - E_{\mathrm{pp}}(\mathbf{x}_i)\right] + \left(\sqrt{\beta_0\beta_i} - \sqrt{\beta_0\beta_j}\right)\left[E_{\mathrm{ps}}(\mathbf{x}_j) - E_{\mathrm{ps}}(\mathbf{x}_i)\right]. \quad (3)$$

Here, $\mathbf{x}_i$ and $\mathbf{x}_j$ are the system configurations of the replicas i and j at the time point of an exchange trial and $\beta = 1/k_BT$, where k_B is Boltzmann's constant.

The exchange prescribed by Eqs. (2, 3) preferentially transfers configurations of low potential energy toward the bottom rung of the temperature ladder (Huang et al. 2007). This bias ensures that the canonical ensembles, which the replicas sample at their respective temperatures, remain undisturbed. Because the helical state of the huH1 peptide is stabilized by strong electrostatic interactions providing an enthalpic barrier to helix unfolding (Morrissey and Shakhnovich 1999; Ziegler et al. 2003), the folded state is expected to preferentially occupy the low temperature rungs. Furthermore, because REST can substantially speed up the sampling of systems with large enthalpic barriers (Zuckerman and Lyman 2006; Denschlag et al 2008), the method should be capable of inducing a substantial number of unfolding events on the time scale of several tens of nanoseconds currently accessible to MD simulations with explicit solvent.

Due to the specific form of the REST potential energy functions Eq. (1), the potential energy of the solvent does not contribute to the exchange probability (2, 3). Therefore, in REST, only 12 replicas are needed to cover the temperature range between 300 and 570 K with reasonable average acceptance probabilities for the exchange. We obtained the following average acceptance probabilities: 22% for H_2O, 25% for H_2O/MeOH and 30% for MeOH. A more detailed analyis of the average exchange probabilities between the individual temperature rungs in the various simulations is available through Fig. s10 and the accompanying text in the supporting information (SI). At comparable average acceptance probabilities, conventional replica exchange would require about 40 replicas to cover the given temperature range (see see van der Spoel et al. 2005; Nadler and Hansmann 2008; Denschlag et al. 2009 for prescriptions on constructing replica exchange temperature ladders for explicit solvent systems).

Note that conventional replica exchange techniques require that the fluctuations of the total potential energy are canonical (Rosta et al 2009). Since the REST exchange probability depends only on the solute energies E_{pp} and E_{sp}, we solely have to guarantee that these energy terms exhibit canonical fluctuations. We have recently shown that the non-invasive strategy of temperature control applied in the present study leads to canonical fluctuations of the solute's kinetic energy (Lingenheil et al. 2008), suggesting that also the fluctuations of E_{pp} and E_{sp} are canonical.

Identification of helical structure

To identify the degree of helicity of a given peptide configuration, we use two different methods. The first one is based on the DSSP classifier by Kabsch and Sander (1983), which identifies helical structure according to typical H-bonding patterns. For a given peptide configuration, we define the DSSP helicity

$$H_{\mathrm{DSSP}} \equiv h/h_{\max}, \quad (4)$$

where h is the number of residues involved in helical structure (3_{10}-helix, α-helix, or π-helix) according to DSSP, and $h_{\max}$ is the number of helical residues for an ideal α-helix. In the case of huH1, $h_{\max} = 11$.

A second helicity measure is based on the ψ-dihedral angles. Residues involved in a helical structure typically have ψ-angles near $\psi_\alpha = -47°$, whereas in an extended structure, the ψ-angle is typically around $\psi_\beta = \psi_\alpha + 180° = 133°$. Figure 1 shows a simple dihedral α-β-scoring function $h_{\mathrm{elo}}(\psi)$, which linearly decreases from 1 to -1 as ψ changes from ψ_α to ψ_β. To measure the helicity in a sequence portion $i \to j$ of the huH1 peptide comprising the residues from i to j, we use the average α-β score

$$H_{\mathrm{elo}}(i \to j) = \frac{\sum_{n=i}^{j} h_{\mathrm{elo}}(\psi_n)}{j - i + 1} \quad (5)$$

of the ψ-dihedral angles $(\psi_i, \ldots, \psi_j)$ within the region $i \to j$. Here, well-formed α-helices are indicated by $H_{\mathrm{elo}} > 0.8$, whereas random coil structures are indicated by values of H_{elo} near zero. To analyze the general behavior of huH1 in terms of helicity, we will use $H_{\mathrm{elo}}^{\mathrm{core}} \equiv H_{\mathrm{elo}}(146 \to 153)$, which measures the helicity of the eight core residues corresponding to the two central rungs of the helical peptide. To get a structurally more resolved insight, we will furthermore analyze our trajectories in terms of the N-terminal helicity-elongation score $H_{\mathrm{elo}}^{\mathrm{N}} \equiv H_{\mathrm{elo}}(146 \to 149)$ and by the C-terminal score $H_{\mathrm{elo}}^{\mathrm{C}} \equiv H_{\mathrm{elo}}(150 \to 153)$. Thus, $H_{\mathrm{elo}}^{\mathrm{core}}$ is the average value of $H_{\mathrm{elo}}^{\mathrm{C}}$ and $H_{\mathrm{elo}}^{\mathrm{N}}$.

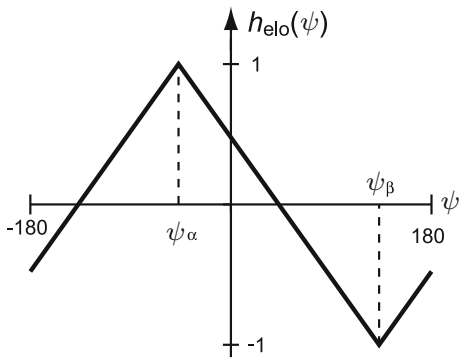

Fig. 1 The dihedral helicity-elongation scoring function $h_{\mathrm{elo}}(\psi)$

Results and discussion

We will now first present our REST simulations of huH1 in pure water and scrutinize the statistical reliability of the results. Subsequently, we will report our observations on the peptide's quite different behavior in the remaining solvents, and, finally, we will examine the contribution of the electrostatic interactions to the differences thus identified.

HuH1 in water is flexible

Our REST simulations H_2O/f and H_2O/u started from completely folded and completely unfolded ensembles, respectively, and thus with grossly different initial conditions. One expects that these initial conditions introduce progressively decaying biases into the conformational ensembles sampled during the simulations. Specifically, we expect the H_2O/f simulation (initially $H_{\mathrm{elo}}^{\mathrm{core}} = 1.0$, $H_{\mathrm{DSSP}} = 1.0$) to be biased toward helical structures and the H_2O/u simulation (initially $H_{\mathrm{elo}}^{\mathrm{core}} = -0.57$, $H_{\mathrm{DSSP}} = 0.0$) toward extended structures. With increasing duration t of the simulations, the biasing influence of the initial conditions will decrease, and we correspondingly expect that the average helicities in the two simulations will (in the long run) both converge toward a common value, measuring the equilibrium helicity of our huH1 computer model.

The progressive decay of the initial helicity bias is illustrated by Fig. 2. Part A of the figure shows the cumulative average $\langle H_{\mathrm{elo}}^{\mathrm{core}}\rangle_t$ of the core helicity-elongation at 300 K as a function of the simulation time t. Immediately after the equilibration ($t = 0$), all replicas are still close to their respective starting structures. Correspondingly, the H_2O/f (solid line) and H_2O/u(dashed line) curves in Fig. 2a start out at $\langle H_{\mathrm{elo}}^{\mathrm{core}}\rangle_0 \approx 0.8$ and $\langle H_{\mathrm{elo}}^{\mathrm{core}}\rangle_0 \approx -0.4$, respectively. During the first 12 ns, the initially folded structures of simulation H_2O/f continuously lose their α-helical character, which is reflected by the marked decrease of the solid line in Fig. 2a. For the remainder of the simulation time, the figure indicates a nearly stationary average helicity-elongation score $\langle H_{\mathrm{elo}}^{\mathrm{core}}\rangle_t \approx 0.35$. Similarly, the H_2O/u structures lose part of their bias toward extended conformations early in the simulation, as indicated by the increase of the dashed line in Fig. 2a up to the random coil value of $\langle H_{\mathrm{elo}}^{\mathrm{core}}\rangle_t \approx 0.0$ during the first 5 ns. For the remaining 35 ns of simulation time, the average helicity-elongation score $\langle H_{\mathrm{elo}}^{\mathrm{core}}\rangle_t$ remains stationary. The fact that the helical structures in simulation H_2O/f decay more slowly than the extended structures in simulation H_2O/u reflects the enthalpic stability provided to the helices by the typical backbone hydrogen bonds and, possibly, additional helix stabilizing mechanisms.

Figure 2b shows a similar analysis of the water results at 300 K in terms of the average helicity $\langle H_{\mathrm{DSSP}}\rangle_t$ as

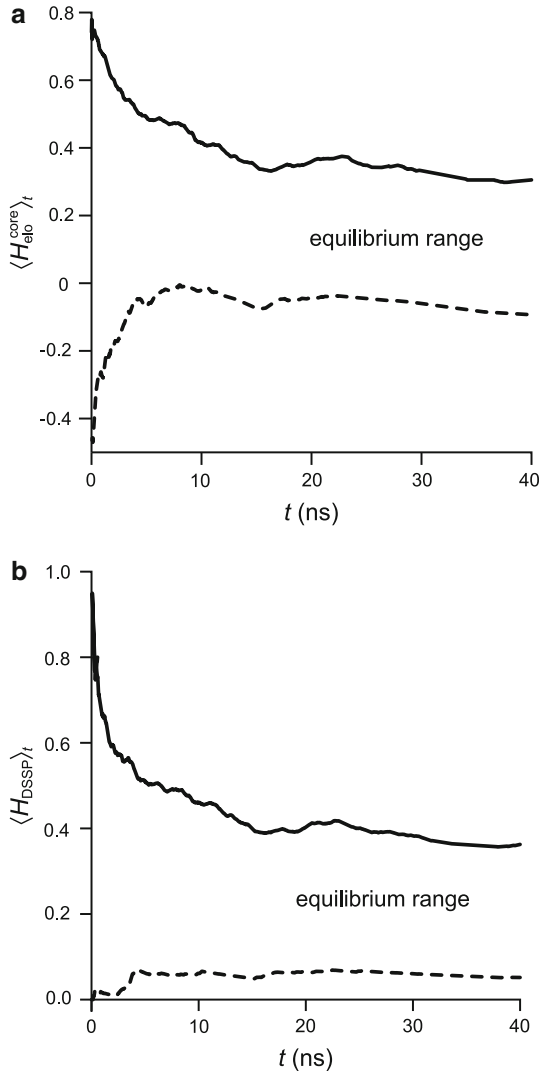

Fig. 2 Average helicity at 300 K plotted as a function of the simulation time t for simulation H_2O/f (*solid lines*) and for simulation H_2O/u (*dashed lines*). **a** Cumulative average helicity-elongation score $\langle H_{\mathrm{elo}}^{\mathrm{core}}\rangle_t$. **b** Cumulative average helicity $\langle H_{\mathrm{DSSP}}\rangle_t$ according to DSSP

measured by DSSP. In agreement with Fig. 2a, also Fig. 2b indicates that the initially α-helical structures of the H_2O/f simulation (solid line) progressively decay for about 15 ns followed by a phase of stationarity. Since the DSSP classifier does not distinguish between extended and random coil structures, the H_2O/u curve (dashed line) does not exhibit a pronounced relaxation phase. Nonetheless, the distinct jump at $t = 4.5$ ns shows that at least one event of helix folding must have occurred early in the simulation.

The considerable gaps between the solid and dashed curves in Fig. 2a and b that remain after 40 ns simulation time are a clear sign of lacking convergence. For a converged sampling of the peptide's folding/unfolding equilibrium, in Fig. 2a and b, the average helicities for H_2O/f

and H_2O/u would have to be equal and, thus, independent of the starting ensemble. However, since the initial helicity biases of the simulations H_2O/f and H_2O/u are extreme, the associated average helicities shown in Fig. 2 are upper and lower bounds for the equilibrium values. Therefore, the equilibrium helicities should be localized somewhere in between the two curves.

According to Fig. 2, the average helicity-elongation of the core residues of huH1 in water is thus between 0.0 and 0.35. These values indicate that the equilibrium ensemble comprises a major random coil component and a minor but probably non-vanishing helical contribution. Similarly, the average equilibrium helicity as classified by DSSP is expected in a range of minimally 7% and maximally 40%. This result nicely agrees with experimental estimates of 7–30% (Ziegler et al. 2003; Fernández et al. 2008) for the total helix content of similar H1 peptides in aqueous solution determined by CD spectroscopy. It furthermore agrees with the 34–42% helical propensities obtained by NMR spectroscopy for the core residues of huH1 in water (Liu et al. 1999).

On the other hand, the REST results displayed by Fig. 2 are at variance with MD results of Dima and Thirumalai (2004) on a peptide covering the sequence portion 144–153 of mouse PrP. These authors analyzed their 90-ns MD trajectories by a helicity measure (Klimov and Thirumalai 2003) comparable to our H_{elo} score and predicted a helical fraction of about 60%. However, since Dima and Thirumalai (2004) started their simulations with a completely helical peptide and employed standard MD at room temperature, one can expect that their simulation remained even more biased toward the initial helical conformation despite a simulation time as long as 90 ns.

Encouraged by the apparent agreement of our REST simulations with the available experimental knowledge, we now will use the complete "virtual reality" provided by these simulations to derive a structurally resolved insight into the folding properties of the H1 sequence. To this end, Fig. 3a displays for the 300-K replica of the H_2O/f simulation the distribution of sampled peptide structures in the plane spanned by the N- and C-terminal helicity-elongation scores H^N_{elo} and H^C_{elo}, respectively. Each sampled structure is represented by a dot. Additionally, the figure shows prototypical peptide conformations characterizing the various regions of the H_{elo}-plane.

The α-helical starting structure of simulation H_2O/f is located in the upper right corner of Fig. 3a, which, therefore, is highly populated. In addition to the folded starting structure, the 300-K replica sampled a variety of partially unfolded conformers. Here, the dominant conformation is α-helical at the N-terminus ($H^N_{elo} > 0.8$) with a partially unfolded C-terminus ($H^C_{elo} \approx 0.4$). Furthermore, as Fig. 3a shows, strictly helical values $H^N_{elo} > 0.8$ for the N-terminal part of the peptide are frequently combined even with negative values of the C-terminal elongation score H^C_{elo}, i.e., with extended C-terminal structures. The inverse situation did not occur in a single instance during the simulation H_2O/f. Thus, the unfolding of the C-terminal end of the helix does not destabilize the N-terminal part of the helix as much as vice versa. Apart from the helical and partially helical conformations neighboring the starting structure in Fig. 3a, the H_2O/f simulation sampled a wide

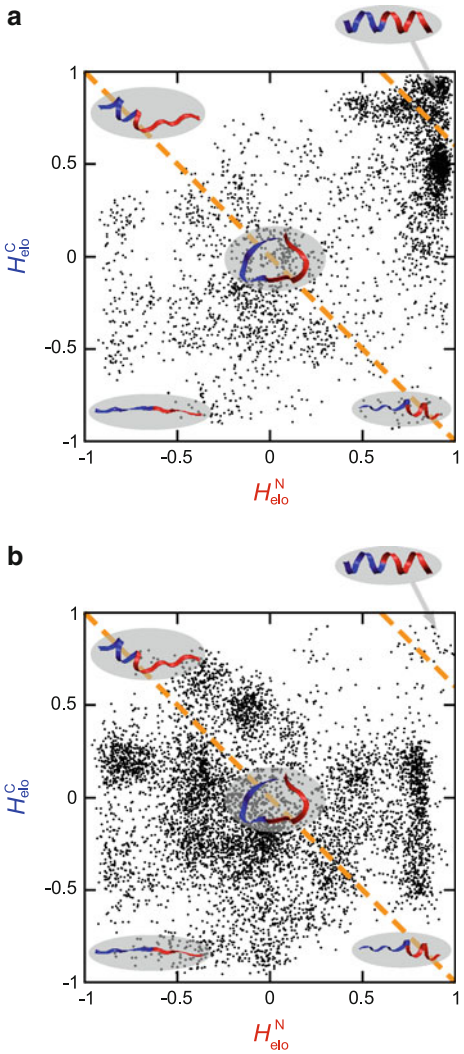

Fig. 3 Distribution of peptide structures in the plane spanned by the N-terminal helicity H^N_{elo} (*red*) and by the C-terminal helicity H^C_{elo} (*blue*) of huH1. *Each dot* represents a snapshot taken every 60 ps from the respective 300-K replica. The five schematic structures of the peptide backbone are prototypical for the various regions of the H_{elo} plane. The *orange dashed lines* indicate borders between peptide conformations. The *upper right line* separates perfect α-helices ($H^{core}_{elo} > 0.8$) from other conformations. The *diagonal line* separates definitely non-helical structures ($H^{core}_{elo} < 0.0$) from conformations with residual helicities. **a** REST simulation H_2O/f. **b** REST simulation H_2O/u

variety of random coil and extended structures, which is illustrated by a considerable and widely scattered population of the central part of the H_{elo} plane.

Figure 3b presents an equivalent diagram for the simulation H_2O/u. The figure is dominated by a large and widely scattered population occupying the center of the H_{elo} plane and indicating random coil conformations. As in Fig. 3a, it is difficult to discern individual clusters of points in this region. Thus, the random coil "conformations" comprise a large number of quickly communicating isoenergetic subconformations. In contrast to the H_2O/f simulation in Fig. 3a, the immediate neighborhood of the starting structure (lower left corner) is not preferentially populated compared with the random coil conformations in the center of the H_{elo} plane. Thus, the initially extended structure rapidly decays in contrast to the initial α-helix of Fig. 3a.

The most striking difference between the two simulations H_2O/f and H_2O/u is, however, that the α-helical region of the H_{elo}-plane in Fig. 3b is sparsely populated, quite in contrast to Fig. 3a. Note furthermore that, in both simulations, we frequently observed structures with a strongly helical N-terminus ($H_{elo}^{N} > 0.8$) and an imperfectly folded C-terminal half ($H_{elo}^{C} < 0.4$). Within simulation H_2O/u this intermediate conformation eventually led in two cases to a fully helical structure. The frequent occurrence of this intermediate is consistent with earlier observations (Liu et al. 1999; Alonso et al. 2002; Dima and Thirumalai 2004; Hirschberger et al. 2006) that the α-helical propensity of the C-terminal part of H1 is somewhat lower than that of the N-terminal part and suggests that the N-terminal residues form a nucleation site for α-helix folding.

Statistical validity and convergence behavior

The populations of the H_{elo} planes in Fig. 3a and 3b differ and show clear signatures of the respective initial conditions. Thus, the comparison of Fig 3a and b once more illustrates that the REST samplings H_2O/f and H_2O/u did not reach convergence within the given time spans of 40 ns. We have observed the lacking convergence already in Fig. 2. Here the helicity averages after 40 ns showed a clear memory of the respective initial conditions. Without a comparison of simulations employing different initial conditions, the fact that the helicity averages in Fig. 2 seem to be nearly stationary for the last 25 ns of the simulations could easily be mistaken as a sign of convergence. However, the observed quasi-stationarity is a typical artifact resulting from an incomplete sampling of a folding/unfolding equilibrium using replica exchange techniques (Denschlag et al. 2008).

We recently introduced a method to asses the statistical validity of RE simulations of peptide folding/unfolding equilibria by counting the number of folding and unfolding events because convergence requires the (multiple) occurrence of such events (Denschlag et al 2008). Our method is based on the following general observation: In replica exchange simulations, each exchange of configurations introduces a discontinuity into the trajectory of a replica i that is simulated at the temperature T_i and whose configuration is modified by the exchange. Therefore, one cannot identify real folding processes by analyzing the trajectories of the replicas at the various temperatures T_i. Instead, one has to consider the continuous trajectories, which move through the temperature space upon exchange and which, for this reason, are termed temperature exchange (TE) replicas. In the given case of the huH1 peptide, we count a folding event if the trajectory of a TE replica makes the complete way from the fully unfolded region ($H_{elo}^{core} < 0.0$) to the fully helical region ($H_{elo}^{core} > 0.8$) in the H_{elo} plane. The borders of these two domains are indicated by the dashed orange lines in Fig. 3. For an unfolding process to be identified, the TE replica has to make the reverse way from the helical to the non-helical domain.

Figure 4 presents the number of folded members defined by this criterion within the ensemble of the 12 TE replicas for the simulations H_2O/f and H_2O/u. In the case of H_2O/f (solid line in Fig. 4), most of the initially α-helical structures decay quickly, leaving only 3 of the initially 12 helices after 10 ns. Due to laws of statistics and the sorting of the enthalpically favorable folded TE replicas to low temperatures (cf. Methods), the unfolding of the next TE replica takes the more time the less folded TE replicas are left (Denschlag et al. 2008). During the 40 ns, the simulation H_2O/f (solid line) showed only three folding events. One TE replica did not unfold at all during the 40-ns simulation and is responsible for the high population of the helical corner in Fig. 3a. In the case of H_2O/u (dashed line in Fig. 4), we observed two folding events. Here, a well-formed α-helix existed for about 3 ns, but eventually unfolded again.

Taken together, Fig. 4 indicates that, although neither the H_2O/f nor the H_2O/u simulation have sufficiently

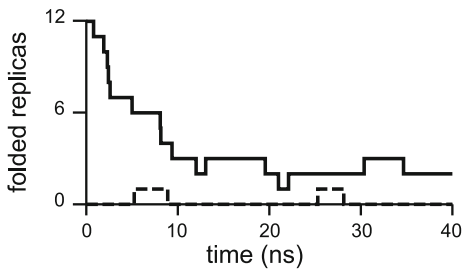

Fig. 4 The number of folded TE replicas as a function of the simulation time for the simulations H_2O/f (*solid line*) and H_2O/u (*dashed line*)

sampled the folding/unfolding equilibrium to derive the exact weights of folded and unfolded conformations in the equilibrium ensemble of huH1, our simulations were long enough to observe several folding events. We thus were able to derive upper (40%) and lower (7%) bounds for the helicity of our huH1 model in TIP3P water at 300 K.

To determine the equilibrium helicity of huH1 in water with greater accuracy, we would have to observe several more folding events. Assuming that the folding time of our computer model of huH1 in the REST setup is somewhere near the 40 ns time span of our simulations, which is plausible given the 2–3 folding events observed in the H_2O simulations, we would have to simulate well above 100 ns to accurately calculate the equilibrium helicity of huH1 in water. Since such an extensive computational effort would not have been feasible for a number of different explicit solvents environments, and because we were mainly interested in the relative kinetic stabilization of the huH1 helix by environments of different polarity, we abstained from further simulating in H_2O for the benefit of three other solvent systems.

The huH1 helix is kinetically stabilized by weakly polar solvents

Figure 5 analyzes the folding/unfolding events of huH1 in different solvents. This analysis is equivalent to the one displayed by Fig. 4 for huH1 in H_2O. For a simplified comparison, the latter data are repeated in panel c. Panels a and b show the results of the REST simulations with the solvents MeOH and the mixture H_2O/MeOH, respectively. Thus, the dielectric constant ε_S (cf. Table 1) of the solvent increases from panel a–c.

As the solid line in panel a indicates, nine helices remained in the MeOH/f simulation after 40 ns of REST. Thus, for the least polar solvent MeOH, the helical conformation is essentially stable on the time scale of our simulation even at temperatures as high as 500 K. Upon increasing the solvent polarity by an admixture of water (solid line, panel b) considerably fewer helices (i.e., 4) survived the unfolding simulation. Finally, and in sharp contrast with the MeOH/f results of panel a, in the highly polar water most helices were unfolded after 40 ns with only two remaining (solid line, panel c). Thus, in our unfolding simulations, the number of unfolded peptides found after 40 ns of REST simulation monotonously increased with increasing solvent polarity. This result suggests that the unfolding kinetics are accelerated by environments of increasing polarity. The fact that the two helices observed in the H_2O/u simulation (dashed line in Fig. 5c) unfolded very quickly after their generation, whereas the two newly formed helices in simulations H_2O/MeOH/u and MeOH/u persisted until the end of the respective simulation further supports our suggestion that helix unfolding seems to be much faster in water than in the other solvents.

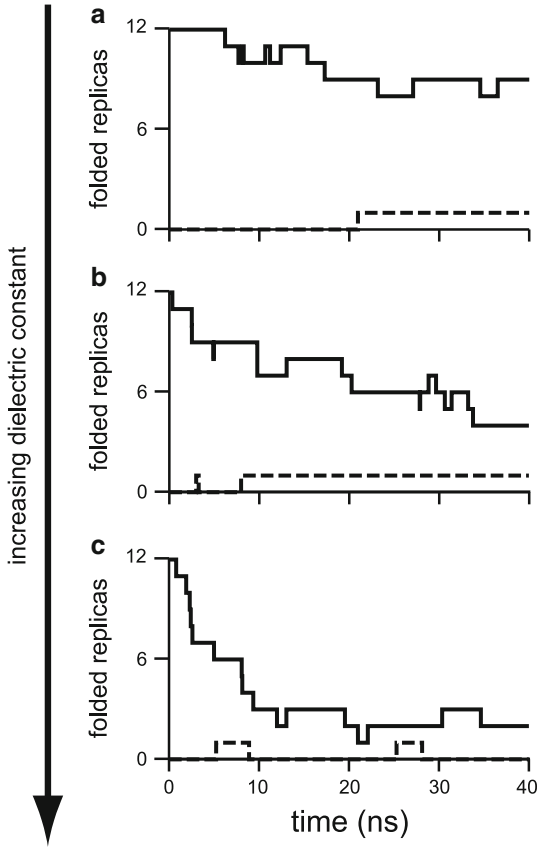

Fig. 5 The number of folded TE replicas as a function of the simulation time. The *line* styles distinguish initial conditions: folded (*solid*) and unfolded (*dashed*). **a** MeOH. **b** H_2O/MeOH. **c** H_2O

With respect to the folding times, the simulations starting from the unfolded ensembles (dashed lines) cannot reveal any significant solvent dependence because the folding of a helix from an unfolded conformation is a rare event on the given 40-ns time scale for all solvents (one event for MeOH, two events for H_2O/MeOH and H_2O each). The apparently quite small folding rates are the main reason for the poor convergence of our REST simulations. Convergence would be guaranteed if these rates could be reliably measured from the simulation data (Denschlag et al. 2008). However, particularly for the weakly polar solvents, such a measurement would require significantly longer simulation times, which are inaccessible to us. The convergence proved even slower in simulations of huH1 in TFE ($\varepsilon_s = 27$, data not shown). This is the reason why we have abstained from a detailed discussion of the results of these simulations, although these results confirm the general trend of increased kinetic helix stability with decreasing ε_s.

Given the poor convergence particularly for the weakly polar solvents (cf. Fig. 5), one may ask the question as to whether there is anything to be learned from such simulations. Clearly, instead of accurate estimates for thermodynamic quantities such as the ratio between folded and unfolded peptides in the equilibrium ensemble, we can only give more or less extended ranges. Nevertheless, these simulations led to two additional and clear-cut conclusions.

The first conclusion pertains to the kinetics of huH1 helix unfolding. The discussion of Fig. 5 has suggested that the unfolding of huH1 is accelerated by solvents of increasing polarity. To quantify this acceleration, we calculated the apparent unfolding times $\tau_u = \langle \tau_i \rangle$ for huH1 in the different solvents. To this end, we determined for every unfolding event i shown in Fig. 5 the time τ_i that the respective TE replica had been folded before. The expected error in τ_u was calculated as $E(\tau_u) = \sigma(\tau_u)/\sqrt{M}$, where M is the number of measurements τ_i, and $\sigma(\tau_u)$ is their standard deviation. For all replicas found folded at the end of the REST simulations, a lower limit of $\tau_i = 40$ ns $- t_i$ for the lifetime was assumed, where t_i denotes the time of the preceding folding event. Thus, the resulting values for τ_u underestimate the actual time needed to unfold a folded helix within our REST setup. This underestimation is the more severe the more replicas are folded at the end of the simulation, which particularly pertains to MeOH (cf. Fig. 5a). Note here that one cannot determine the mean unfolding times at 300 K from the apparent unfolding times τ_u observed in our REST simulations because the latter times refer to a temperature-activated process and, therefore, are probably much shorter than the former. However, the ratios of the REST unfolding times in the different solvents should be measures for the corresponding ratios at 300 K.

Table 2 shows the REST unfolding times τ_u of huH1 obtained for the various solvents. According to the data, τ_u significantly decreases with increasing solvent polarity. For instance, for MeOH the REST unfolding time τ_u is at least 1.7 times larger than for water, showing that the unfolding energy barrier is significantly larger in MeOH. It is plausible that the delayed unfolding of the helical conformation of the H1 sequence, i.e., the larger kinetic stability, is also responsible for the enhanced thermodynamic stability of the helix conformation observed experimentally for H1 peptides in organic solvents (Sharman et al 1998; Liu et al. 1999; Thompson et al. 2000; Tahiri-Alaoui et al. 2003; Ziegler et al. 2003; Megy et al. 2004).

Table 2 Mean REST unfolding times τ_u of huH1 in the different solvents. $E(\tau_u)$ denotes the estimated error

Solvent	τ_u (ns)	$E(\tau_u)$ (ns)	M
MeOH	22.7	3.7	18
H_2O/MeOH	15.0	3.1	19
H_2O	8.1	2.8	17

M denotes the size of the samples entering the calculations

As outlined in the Introduction, the main objective of this study was to answer the question whether the α-helical conformation of the H1 sequence as found in PrP^C is more likely to unfold, once the S1–H1–S2 domain becomes separated from the hydrophobic core of the protein, thereby bringing H1 from an environment with a low dielectric constant into one with a high dielectric constant. The fact that the REST unfolding rates in Table 2 strictly increase with increasing solvent polarity indicates that this is indeed the case, if the ratios of the REST unfolding times τ_u (cf. Table 2) qualitatively represent the corresponding ratios at 300 K.

Helical huH1 has a specifically low potential energy

The second conclusion that can be derived from our REST simulations pertains to the energetics of the huH1 peptide. This energetics is revealed by the distribution of helical conformations along the temperature ladder. As an example, Fig. 6 shows the average DSSP helix fraction observed at the 12 rungs of the temperature ladder during the last 30 ns of the simulations H_2O/MeOH/f (circles) and H_2O/MeOH/u (squares). Similar comparisons for the other solvents are presented as in Fig. s11 of the SI. If convergence were achieved, the helicities would have to be independent of the initial conditions. Conversely, the size of the gap between the two curves in Fig. 6 indicates how far our simulations deviate from convergence at the various

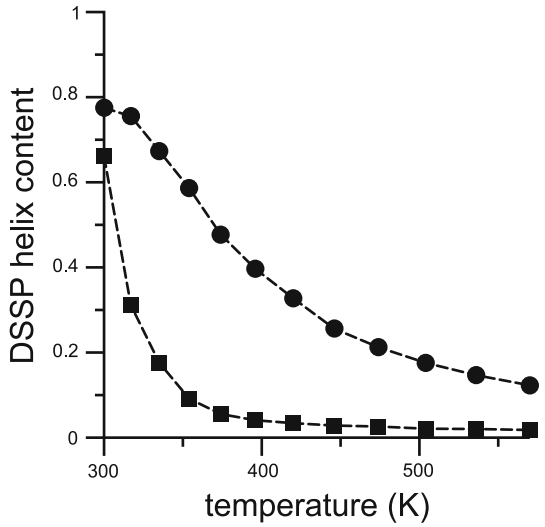

Fig. 6 Average helical content according to DSSP observed during the final 30 ns of the simulation H_2O/MeOH/f (*circles*) and H_2O/MeOH/u (*squares*) as a function of the temperature

temperatures. At the 300-K target temperature of the REST sampling, the two curves for H_2O/MeOH/f and H_2O/MeOH/u in Fig. 6 are very close to each other, indicating a helix fraction between 67 and 79%. Furthermore, in simulation H_2O/MeOH/u (squares), the helical content of the REST ensemble is essentially confined to the three lowest temperature rungs. Recall that this simulation showed only one folding event leading to a stable helix (cf. the dashed curve in Fig. 5b).

Figure 7 illustrates the distributions of folded and unfolded states observed during the REST simulation H_2O/MeOH/u. Figure 7a pertains to the single TE replica that underwent the folding into a stable helix. The figure shows the random walk of this replica on the temperature ladder and demonstrates that, after folding (gray shaded area), the replica remained confined to the lowest temperature rungs. In contrast, the random walk of an unfolded replica (Fig. 7b) rarely visits these rungs, while moving freely along the remainder of the ladder.

Now recall that the Metropolis exchange criterion given by Eqs. (2, 3) preferentially moves structures with low potential energies to low temperatures. Hence, the pronounced sorting of the helical replica in simulation H_2O/MeOH/u clearly demonstrates that its helical conformation is characterized by a very low potential energy compared with the unfolded conformations of the other replicas (Huang et al. 2007). The strong sorting of helical structures to low temperatures is also evident from the monotonous decrease of the helicity profiles shown for H_2O/MeOH in Fig. 6 and for the other solvents in Fig. s11 of the SI. Thus, the average potential energy of the α-helical states must be much lower than those of the unfolded states.

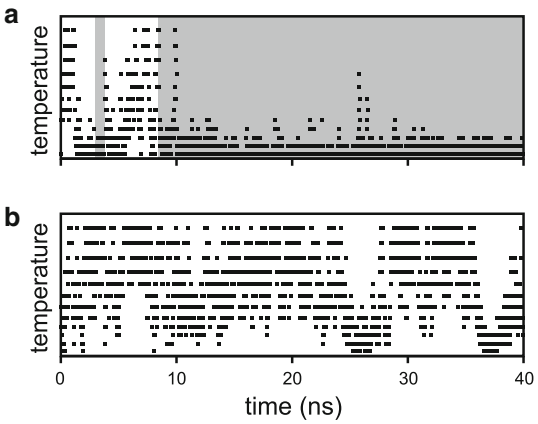

Fig. 7 The random walks performed by two replicas in the H_2O/MeOH/u simulation. The position of the replica on the temperature ladder is indicated by a square in intervals of 200 ps. **a** A TE replica that undergoes folding transitions. The lifetime of the helix is indicated by a *gray background*. **b** A TE replica that remains unfolded during the simulation

The role of electrostatic interactions

Various studies have previously indicated that the stability of H1 in PrP and H1 peptides is dominantly caused by electrostatic interactions (Morrissey and Shakhnovich 1999; Ziegler et al. 2003; Fernández et al. 2008; Megy et al. 2004; Dima and Thirumalai 2004). Thus, these interactions are the likely cause for the kinetic stabilization of the huH1 helix. To check this issue, we now consider the electrostatics of the folded state in more detail.

Like every α-helix, also that of huH1 is stabilized by hydrogen bonds within the backbone. However, as schematically shown by Fig. 8, the H1 sequence enables four favorable $i, i + 4$ salt bridges (Asp^{144}-Arg^{148}, Asp^{147}-Arg^{151}, Arg^{148}-Glu^{152} and Glu^{152}-Arg^{156}) (Morrissey and Shakhnovich 1999; Ziegler et al. 2003; Fernández et al. 2008; Megy et al. 2004; Dima and Thirumalai 2004; Speare et al. 2003; De Simone et al. 2007). The total dipole moment generated by the ionic groups in the huH1 helix is directed antiparallel to the macrodipole generated by the the backbone peptide groups and, thus, lowers the electrostatic energy.

The core of the helix is dominated by a quadrupolar motif (Fernández et al. 2008) composed of Asp^{147}, Arg^{148}, Arg^{151} and Glu^{152}. The associated quadrupole field is short-ranged and, therefore, the solvent's dielectric properties cannot strongly alter the potential energy of the quadrupolar charge group. However, during unfolding, the charges making up the quadrupole must become separated and solvated, which is is energetically favored in highly polar solvents. Thus, in weakly polar solvents, the enthalpic barrier towards unfolding should have a large

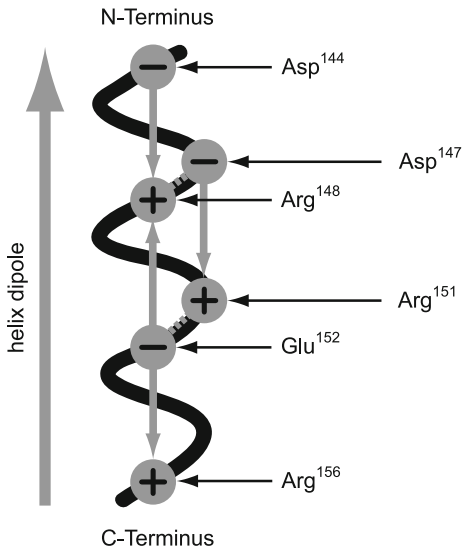

Fig. 8 Schematic representation of the electrostatic network in the α-helical conformation of huH1

contribution associated with the breaking of the $i, i + 4$ salt bridges. As a result, the apparent lifetime of the folded state in our REST simulations (cf. Table 2) should correlate with the frequency f_{sb} of salt bridges observed in this state.

To check whether such a correlation exists, we analyzed whether the four potential $i, i + 4$ salt bridges in huH1 were realized whenever the peptide backbone connecting the two residues was classified as α-helical by DSSP, i.e., if the typical backbone hydrogen bonds were present. The existence of a salt bridge was assumed if the distance d of the C-atoms in the guanidinium and the carboxylate ionic groups of the respective residues was less than 5 Å. The analysis was performed for every solvent using the 300-K replicas of the simulations starting with folded ensembles.

Figure 9 demonstrates the expected correlation between the mean REST unfolding time τ_u of the helix and the relative frequency f_{sb} of the salt bridges in the helical state. In water, the ions are solvated most of the time ($f_{sb} = 21\%$). Hence, the unfolding of the helix does not additionally require the breaking of salt bridges and the REST unfolding rate is correspondingly large. The solvation of the ions becomes less and less favorable with decreasing solvent polarity. Then, the salt bridges become stable and provide an additional energy barrier to the unfolding of the connecting helical turn. Hence, the sketched mechanism certainly contributes to the observed delayed unfolding of the helix in weakly polar solvents. We conclude that the free energy required for the unfolding transition must be dominated by the enthalpy for the breakup of the intricate network of electrostatic interactions shown in Fig. 8.

To obtain a microscopic insight into the interactions of the peptide with the solvent molecules and, thus, into the reason for the different kinetics, we investigated the solvation of the charged side chains for the different solvents and peptide conformations. Fig. s12 of the SI shows the radial distribution of the solvent around the side chain anions. The figure demonstrates that the solvation of the anionic side chains in H_2O is independent of the folding state of the peptide. In MeOH, however, the solvation of the side chains is about 20% smaller for the unfolded states than for the helix, suggesting that additional *intra*-peptide salt bridges replace some solute-solvent interactions upon unfolding.

To check whether the formation of salt bridges is actually more common in the unfolded than in the folded state, we calculated the average numbers of salt bridges for H_2O and MeOH and the two conformational states considering all possible (i.e., 12) combinations of oppositely charged residues. Further above we had seen that in MeOH and in the helical state, the probability for the formation of the typical $i, i + 4$ salt bridges is very high (65%, cf. Fig. 9). Our counting has now shown that the non-helical configurations in MeOH exhibit an average of 3.5 salt bridges, whereas in the helical state only 2.6 salt bridges are formed. In contrast, for H_2O, the average number of salt bridges is always small with 0.7 (non-helical) and 0.8 (helical), respectively. Consequently, in MeOH the non-helical configurations are even more strongly stabilized by salt bridges than the helical ones. The prevalence of many enthalpically stabilized unfolded conformations is likely the reason for the slow folding/unfolding dynamics in MeOH and thus for the slow convergence toward equilibrium.

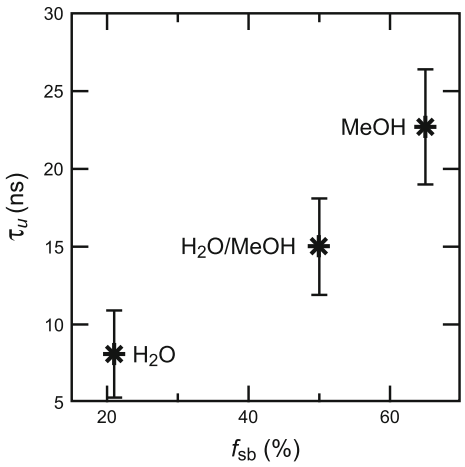

Fig. 9 The mean REST unfolding time τ_u plotted over the relative frequency f_{sb} of $i, i + 4$ salt bridges in the helical state

Temperature mixing

The strong sorting of folded replicas toward the lowest rungs of the REST temperature ladder illustrated by Fig. 7 may have reduced the efficiency of our REST simulations. For REST to be optimally efficient, all replicas should cycle as rapidly as possible from low to high temperatures and back again (Katzgraber et al. 2006; Huang et al 2007; Nadler et al. 2008). To gain some clarity with respect to this point, we checked the mixing behavior of our simulations by calculating the average number N_r of round trips performed by the TE replicas for the various simulations. The results of these calculations are given in Table 3 and demonstrate that the mixing is strongly impeded in the weakly polar solvents compared with water. Also, N_r is always larger for the simulation starting with an unfolded ensemble than when starting with a folded ensemble.

It is important to note that the weak mixing in H_2O/MeOH and MeOH does not become evident from a simple inspection of the average exchange probabilities p_{acc} for the different simulations shown in Fig. s10 in the SI. Although p_{acc} varies somewhat over the temperature ladder

Table 3 Average number N_r of round trips per TE replica observed for the various simulations

Folded		Unfolded	
Solvent	N_r	Solvent	N_r
H_2O	21	H_2O	23
H_2O/MeOH	5	H_2O/MeOH	9
MeOH	3	MeOH	5

for all solvents, it is not possible to identify any "bottleneck" regions on the ladders with a greatly reduced p_{acc}.

However, the fact that p_{acc} is approximately constant and sizeable is not sufficient to ensure good temperature mixing (Katzgraber et al. 2006; Nadler et al. 2008). Although p_{acc} in MeOH exceeds the value in H_2O by nearly a factor of 1.5, the random walks in MeOH still are strongly confined (see Table 3), probably due to a large potential energy gap between the peptide's different conformations (Huang et al. 2007). The enhanced formation of salt bridges with decreasing solvent polarity demonstrated above is the most likely reason for this effect, which may explain the weak convergence particularly of our MeOH simulations.

As pointed out by Huang et al. (2007), using conventional replica exchange may be superior to REST in such a situation. To still allow for the efficient REST simulation of huH1 and other systems exhibiting such a temperature mixing problem, one should consider the application of feedback-optimized temperature ladders (Katzgraber et al. 2006; Nadler et al. 2008) or of a modified REST scheme, which includes some of the water molecules into the unscaled part of the simulation system (Huang et al. 2007).

Summary

The role of helix 1 in the conversion of the prion protein from the cellular isoform PrP^C to the scrapie isoform PrP^{Sc} has been discussed ever since the NMR structure of PrP^C has been published. H1 has been suggested to unfold during the conversion of PrP^C to PrP^{Sc} (Govaerts et al. 2004; Stork et al. 2005; Langedijk et al. 2006). If an unfolding of H1 is necessary, the stability of the helical conformation of H1 is a key to the question whether H1 constitutes a barrier (Ziegler et al. 2003) for the conversion of PrP^C to PrP^{Sc} or rather a weak point (Hirschberger et al. 2006) at which this conversion starts. Furthermore, the evidence (Norstrom and Mastrianni 2006; Watzlawik et al. 2006; Solforosi et al. 2007; Yu et al 2007; Hesp et al. 2007) for the H1 region to be involved in the binding of PrP^C to PrP^{Sc} immediately leads to the question whether, during this process, the helix remains firmly folded and thus is a passive player or whether it plays an active part due to conformational flexibility.

In our simulations of the huH1 peptide, we observed that the isolated H1 sequence is dominantly non-helical in water. A DSSP analysis of the sampled peptide structures indicates a helical content in a range of 7–40%, consistent with experimental values for H1 peptides in water (Ziegler et al. 2003; Fernández et al 2008). Furthermore, we observed that the helical conformation of huH1 is strongly stabilized against unfolding by weakly polar solvents (such as methanol or TFE), which is also consistent with experimental data (Megy et al. 2004; Sharman et al. 1998; Liu et al 1999; Thompson et al. 2000; Tahiri-Alaoui et al. 2003; Ziegler et al 2003). In our REST simulations, an increasing kinetic stabilization of the helical conformation of huH1 was strongly correlated with a decreasing polarity of the environment as measured by the dielectric constant.

The specific distribution of charged residues in the sequence of H1 leads to a very low electrostatic energy of the α-helical state in weakly polar environments. If the conversion of PrP^C to PrP^{Sc} requires the unfolding of H1, the stability of this helix will indeed represent a barrier as long as it is confined to a low-dielectric environment. However, in a highly polar environment such as bulk water, the efficient screening of the electrostatic interactions reduces the electrostatic stabilization of the helix, thereby lowering the unfolding barrier. The unusual electrostatics of the H1 sequence can also explain why H1 peptides are extraordinarily sensitive environmental switches that assume a helical conformation in weakly polar environments and are predominantly non-helical in bulk water (Megy et al. 2004; Sharman et al. 1998; Liu et al. 1999; Thompson et al. 2000; Tahiri-Alaoui et al. 2003; Ziegler et al. 2003; Fernández et al. 2008).

For an H1 sequence embedded into the prion protein, the kinetic stability of the helix will also be steered by the polarity of the environment. Thus, any conformational fluctuation that brings H1 from the low-dielectric protein surface into the bulk solvent will catalyze its unfolding. There are a number of reasons to assume that H1 may become separated from the hydrophobic core of PrP^C early in the conversion process to PrP^{Sc} (Calzolai and Zahn 2003; Schwarzinger et al 2006; Hirschberger et al. 2006; Eghiaian et al. 2007; De Simone et al 2007; Gsponer et al. 2001; Alonso et al. 2002; Levy and Becker 2002; Colacino et al. 2006; Pappalardo et al. 2007). Then the helix will face a considerably more polar environment, and its unfolding will become much more likely.

In a subsequent step, the unfolded H1 region may take part in a specific interaction with a binding partner (Norstrom and Mastrianni 2006; Watzlawik et al. 2006; Solforosi et al. 2007; Yu et al. 2007; Hesp et al. 2007). Here, a potential binding partner would have to offer a peculiar electrostatic environment that can efficiently compete with the $i, i + 4$ salt bridges, potentially promoting

the formation of a H1 helix. In this respect, it is interesting to note that the exact distribution of positive and negative charges within H1 seems to be quite important for the conversion efficiency of PrP^{C} to the pathogenic PrP^{Sc} (Norstrom and Mastrianni 2006).

Acknowledgments This work was supported by the Bavarian joint research project ForPrion (LMU02) and by Deutsche Forschungsgemeinschaft (SFB533/C1, SFB749/C4). Access to the resources of the Leibniz-Rechenzentrum HPC Linux Cluster (project UH408) is gratefully acknowledged.

References

Allen MP, Tildesley DJ (1987) Computer simulations of liquids. Oxford University Press, Oxford

Alonso DOV, Cham A, Daggett V (2002) Simulations of biomolecules: characterization of the early steps in the ph-induced conformational conversion of the hamster, bovine and human forms of the prion protein. Phil Trans R Soc Lond A 360:1165–1178

Berendsen HJC, Postma JPM, van Gunsteren WF, Di Nola A, Haak JR (1984) Molecular dynamics with coupling to an external bath. J Chem Phys 81:3684–3690

Calzolai L, Zahn R (2003) Influence of ph on nmr structure and stability of the human prion protein globular domain. J Biol Chem 278:35592–35596

Caughey BW, Dong A, Bhat KS, Ernst D, Hayes SF, Caughey WS (1991) Secondary structure-analysis of the scrapie-associated protein prp 27-30 in water by infrared-spectroscopy. Biochemistry 30:7672–7680

Cobb NJ, Sönnichsen FD, Mchaourab H, Surewicz WK (2007) Molecular architecture of human prion protein amyloid: a parallel, in-register β-structure. Proc Natl Acad Sci USA 104:18946–18951

Cohen FE, Pan KM, Huang Z, Baldwin M, Fletterick RJ, Prusiner SB (1994) Structural clues to prion replication. Science 264:530–531

Colacino S, Tiana G, Broglia RA, Colombo G (2006) The determinants of stability in the human prion protein: insights into folding and misfolding from the analysis of the change in the stabilization energy distribution in different conditions. Prot Struct Funct Bioinf 62:698–707

De Simone A, Zagari A, Derreumaux P (2007) Structural and hydration properties of the partially unfolded states of the prion protein. Biophys J 93:1284–1292

DeMarco ML, Daggett V (2004) From conversion to aggregation: Protofibril formation of the prion protein. Proc Natl Acad Sci USA 101:2293–2298

Denschlag R, Lingenheil M, Tavan P (2008) Efficiency reduction and pseudo-convergence in replica exchange sampling of peptide folding-unfolding equilibria. Chem Phys Lett 458:244–248

Denschlag R, Lingenheil M, Tavan P (2009) Optimal temperature ladders on replica exchange. Chem Phys Lett 473:193–195

Dima RI, Thirumalai D (2004) Probing the instabilities in the dynamics of helical fragments from mouse PrP^{C}. Proc Natl Acad Sci USA 101:15335–15340

Eghiaian F, Daubenfeld T, Quenet Y, van Audenhaege M, Bouin AP, van der Rest G, Grosclaude J, Rezaei H (2007) Diversity in prion protein oligomerization pathways results from domain expansion as revealed by hydrogen/deuterium exchange and disulfide linkage. Proc Natl Acad Sci USA 104:7414–7419

Eichinger M, Grubmuller H, Heller H, Tavan P (1997) Famusamm: an algorithm for rapid evaluation of electrostatic interactions in molecular dynamics simulations. J Comput Chem 18:1729–1749

Eigen M (1996) Prionics or the kinetic basis of prion diseases. Biophys Chem 63:A1–A18

Fernández A, Crespo A, Maddipati S, Scott R (2008) Bottom-up engineering of peptide cell translocators based on environmentally modulated quadrupole switches. ACS Nano 2:61–68

Govaerts C, Wille H, Prusiner SB, Cohen FE (2004) Evidence for assembly of prions with left-handed β-helices into trimers. Proc Natl Acad Sci USA 101:8342–8347

Griffith JS (1967) Self-replication and scrapie. Nature 215:1043–1044

Gsponer J, Ferrara P, Calfisch A (2001) Flexibility of the murine prion protein and its Asp178Asn mutant investigated by molecular dynamics simulations. J Mol Graphics Modell 20:169–182

Hesp JR, Raven NDH, Sutton JM (2007) A role for His155 in binding of human prion peptide 144–167 to immobilised prion protein. Biochem Biophys Res Commun 362:695–699

Hirschberger T, Stork M, Schropp B, Winklhofer KF, Tatzelt J, Tavan P (2006) Structural instability of the prion protein upon M205S/R mutations revealed by molecular dynamics simulations. Biophys J 90:3908–3918

Huang XH, Hagen M, Kim B, Friesner RA, Zhou RH, Berne BJ (2007) Replica exchange with solute tempering: efficiency in large scale systems. J Phys Chem B 111:5405–5410

Jamin N, Coic YM, Landon C, Ovtracht L, Baleux F, Neumann JM, Sanson A (2002) Most of the structural elements of the globular domain of murine prion protein form fibrils with predominant beta-sheet structure. FEBS Lett 529:256–260

Jarrett JT, Lansbury Jr PT (1993) Seeding "one-dimensional crystallization" of amyloid: a pathogenic mechanism in Alzheimer's disease and scrapie? Cell 73:1055–1058

Ji HF, Zhang HY, Shen LA (2005) The role of electrostatic interaction in triggering the unraveling of stable helix 1 in normal prion protein. A molecular dynamics simulation investigation. J Biomol Struct Dyn 22:563–570

Jorgensen WL, Chandrasekhar J, Madura JD, Impey RW, Klein ML (1983) Comparison of simple potential functions for simulating liquid water. J Chem Phys 79:926–935

Kabsch W, Sander C (1983) Dictionary of protein secondary structure: pattern recognition of hydrogen-bonded and geometrical features. Biopolymers 22:2577–2637

Katzgraber HG, Trebst S, Huse DA, Troyer M (2006) Feedback-optimized parallel tempering Monte Carlo. J Stat Mech P03018:1742–5468

Klimov DK, Thirumalai D (2003) Dissecting the assembly of a beta(16–22) amyloid peptides into antiparallel beta sheets. Structure 11:295–307

Kozin SA, Bertho G, Mazur AK, Rabesona H, Girault JP, Haertle T, Takahashi M, Debey P, Hoa GHB (2001) Sheep prion protein synthetic peptide spanning helix 1 and beta-strand 2 (residues 142–166) shows beta-hairpin structure in solution. J Biol Chem 276:46364–46370

Kraeutler V, van Gunsteren WF, Hünenberger PH (2001) A fast SHAKE algorithm to solve distance constraint equations for small molecules in molecular dynamics simulations. J Comput Chem 22:501–508

Langedijk JPM, Fuentes G, Boshuizen R, Bonvin AMJJ (2006) Two-rung model of a left-handed β-helix for prions explains species barrier and strain variation in transmissible spongiform encephalopathies. J Mol Biol 360:907–920

Levy Y, Becker OM (2002) Conformational polymorphism of wild-type and mutant prion proteins: energy landscape analysis. Prot Struct Funct Genet 47:458–468

Lingenheil M, Denschlag R, Reichold R, Tavan P (2008) The "hot-solvent/cold-solute" problem revisited. J Chem Theory Comput 4:1293–1306

Liu AZ, Riek P, Zahn R, Hornemann S, Glockshuber R, Wuthrich K (1999) Peptides and proteins in neurodegenerative disease: helix propensity of a polypeptide containing helix 1 of the mouse prion protein studied by NMR and CD spectroscopy. Biopolymers 51:145–152

Liu P, Kim B, Friesner RA, Berne BJ (2005) Replica exchange with solute tempering: a method for sampling biological systems in explicit water. Proc Natl Acad Sci USA 102:13749–13754

Lu X, Wintrode PL, Surewicz WK (2007) β-sheet core of human prion protein amyloid fibrils as determined by hydrogen/deuterium exchange. Proc Natl Acad Sci USA 104:1510–1515

MacKerell AD Jr, Feig M, Brooks CL III (2004) Extending the treatment of backbone energetics in protein force fields: limitations of gas-phase quantum mechanics in reproducing protein conformational distributions in molecular dynamics simulations. J Comput Chem 25:1400–1415

MacKerell AD, Bashford D, Bellott M, Dunbrack RL, Evanseck JD, Field MJ, Fischer S, Gao J, Guo H, Ha S, Joseph-McCarthy D, Kuchnir L, Kuczera K, Lau FTK, Mattos C, Michnick S, Ngo T, Nguyen DT, Prodhom B, Reiher WE, Roux B, Schlenkrich M, Smith JC, Stote R, Straub J, Watanabe M, Wiorkiewicz-Kuczera J, Yin D, Karplus M (1998) All-atom empirical potential for molecular modeling and dynamics studies of proteins. J Phys Chem B 102:3586–3616

Mathias G, Egwolf B, Nonella M, Tavan P (2003) A fast multipole method combined with a reaction field for long-range electrostatics in molecular dynamics simulations: the effects of truncation on the properties of water. J Chem Phys 118:10847–10860

Megy S, Bertho G, Kozin SA, Debey P, Hoa GHB, Girault JP (2004) Possible role of region 152–156 in the structural duality of a peptide fragment from sheep prion protein. Protein Sci 13:3151–3160

Morrissey MP, Shakhnovich EI (1999) Evidence for the role of PrP^C helix 1 in the hydrophilic seeding of prion aggregates. Proc Natl Acad Sci USA 96:11293–11298

Mukherjee LM, Grunwald E (1958) Physical properties and hydrogen bonding in the system ethanol-2,2,2-trifluoroethanol. J Phys Chem 62:1311–1314

Munoz V, Serrano L (1994) Elucidating the folding problem of helical peptides using empirical parameters. Nature Struct Biol 1:399–409

Munoz V, Serrano L (1995) Elucidating the folding problem of helical peptides using empirical parameters. II. Helix macrodipole effects and rational modification of the helical content of natural peptides. J Mol Biol 245:275–296

Nadler W, Hansmann UHE (2008) Optimized explicit-solvent replica exchange molecular dynamics from scratch. J Phys Chem B 112:10386–10387

Nadler W, Meinke JH, Hansmann UHE (2008) Folding proteins by first-passage-times-optimized replica exchange. Phys Rev E 78:061905

Nelson JW, Kallenbach NR (1986) Stabilization of the ribonuclease s-peptide α-helix by trifluoroethanol. Prot Struct Funct Genet 1:211–217

Niedermeier C, Tavan P (1996) Fast version of the structure adapted multipole method-efficient calculation of electrostatic forces in protein dynamics. Mol Simul 17:57–66

Norstrom EM, Mastrianni JA (2006) The charge structure of helix 1 in the prion protein regulates conversion to pathogenic PrP^{Sc}. J Virol 80:8521–8529

Pan KM, Baldwin M, Nguyen J, Gasset M, Serban A, Groth D, Mehlhorn I, Huang ZW, Fletterick RJ, Cohen FE, Prusiner SB (1993) Conversion of α-helices into β-sheets features in the formation of the scrapie prion proteins. Proc Natl Acad Sci USA 90:10962–10966

Pan T, Chang BG, Wong P, Li CY, Li RL, Kang SC, Robinson JD, Thompsett AR, Tein P, Yin SM, Barnard G, McCconnell I, Brown DR, Wisniewski T, Sy MS (2005) An aggregation-specific enzyme-linked immunosorbent assay: detection of conformational differences between recombinant PrP protein dimers and PrP^{Sc} aggregates. J Virol 79:12355–12364

Pankiewicz J, Prelli F, Sy MS, Kascsak RJ, Kascsak RB, Spinner DS, Carp RI, Meeker HC, Sadowski M, Wisniewski T (2006) Clearance and prevention of prion infection in cell culture by anti-PrP antibodies. Eur J Neurosci 23:2635–2647

Pappalardo M, Milardi D, Grasso D, La Rosa C (2007) Steered molecular dynamics studies reveal different unfolding pathways of prions from mammalian and non-mammalian species. New J Chem 31:901–905

Prusiner SB (1982) Novel proteinaceous infectious particles cause scrapie. Science 216:136–144

Prusiner SB (1998) Prions. Proc Natl Acad Sci USA 95:13363–13383

Reichold R (2009) Rechnergestützte Beschreibung der Struktur und Dynamik von Peptiden und ihren Bausteinen. Doktorarbeit, Fakultät für Physik, LMU München

Rosta E, Buchete NV, Hummer G (2009) Thermostat artifacts in replica exchange molecular dynamics simulations. J Chem Theory Comput 5:1393–1399

Schaftenaar G, Noordik J (2000) Molden: a pre- and post-processing program for molecular and electronic structures. J Comput Aid Mol Des 14:123–134

Schwarzinger S, Horn AHC, Ziegler J, Sticht H (2006) Rare large scale subdomain motions in prion protein can initiate aggregation. J Biomol Struct Dyn 23:581–590

Sharman GJ, Kenward N, Williams HE, Landon M, Mayer RJ, Searle MS (1998) Prion protein fragments spanning helix 1 and both strands of beta sheet (residues 125–170) show evidence for predominantly helical propensity by CD and NMR. Fold Des 3:313–320

Shen M, Freed KF (2002) Long time dynamics of Met-Enkephalin: comparison of explicit and implicit solvent models. Biophys J 82:1791–1808

Shoemaker KR, Kim PS, York EJ, Stewart JM, Baldwin RL (1987) Tests of the helix dipole model for stabilization of α-helices. Nature 326:563–567

Solforosi L, Bellon A, Schaller M, Cruite JT, Abalos GC, Williamson RA (2007) Toward molecular dissection of prpc-prpsc interaction. J Biol Chem 282:7465–7471

Speare JO, Rush TS, Bloom ME, Caughey B (2003) The role of helix 1 aspartates and salt bridges in the stability and conversion of prion protein. J Biol Chem 278:12522–12529

Stork M, Giese A, Kretzschmar HA, Tavan P (2005) Molecular dynamics simulations indicate a possible role of parallel β-helices in seeded aggregation of poly-Gln. Biophys J 88:2442–2451

Surewicz WK, Jones EM, Apetri AC (2006) The emerging principles of mammalian prion propagation and transmissibility barriers: insight from studies in vitro. Acc Chem Res 39:654–662

Tahiri-Alaoui A, Bouchard M, Zurdo J, James W (2003) Competing intrachain interactions regulate the formation of beta-sheet fibrils in bovine PrP peptides. Protein Sci 12:600–608

Thompson A, White AR, McLean C, Masters CL, Cappai R, Barrow CJ (2000) Amyloidgenicity and neurotoxicity of peptides corresponding to the helical regions of PrP^C. J Neurosci Res 62:293–301

van der Spoel D, Lindahl E, Hess B, van Buuren AR, Apol E, Meulenhoff PJ, Tieleman DP, Sijbers ALTM, Feenstra KA, van Drunen R, Berendsen HJC (2005) Gromacs User Manual version 3.3. http://www.gromacs.org

Walser R, Mark AE, van Gunsteren WF (1999) On the validity of Stoke's law at the molecular level. Chem Phys Lett 303:583–586

Walser R, Mark AE, van Gunsteren WF (2000) The effect of force-field parameters on properties of liquids: parametrization of a simple three-site model for methanol. J Chem Phys 112:10450–10459

Watzlawik J, Skora L, Frense D, Griesinger C, Zweckstetter M, Schulz-Schaeffer WJ, Kramer ML (2006) Prion protein helix 1 promotes aggregation but is not converted into beta-sheet. J Biol Chem 281:30242–30250

Wille H, Prusiner SB (1999) Ultrastructural studies on scrapie prion protein crystals obtained from reverse micellar solutions. Biophys J 76:1048–1062

Williamson RA, Peretz D, Pinilla C, Ball H, Bastidas RB, Rozenshteyn R, Houghten RA, Prusiner SB, Burton DR (1998) Mapping the prion protein using recombinant antibodies. J Virol 72:9413–9418

Wohlfarth C (2008) Static dielectric constants of pure liquids and binary liquid mixtures, Landolt-Börnstein: numerical data and functional relationships in science and technology-new series. Physical Chemistry, vol 17. Springer, London

Wüthrich K, Riek R (2001) Three-dimensional structures of prion proteins. Adv Protein Chem 57:55–82

Yu S, Yin S, Li C, Wong P, Chang B, Xiao F, Kang SC, Yan H, Xiao G, Tien P, Sy MS (2007) Aggregation of prion protein with insertion mutations is proportional to the number of inserts. Biochem J 403:343–351

Zahn R, Liu A, Lührs T, Riek R, von Schroetter C, López-García F, Billeter M, Calzolai L, Wider G, Wüthrich K (2000) NMR solution structure of the human prion protein. Proc Natl Acad Sci USA 97:145–150

Ziegler J, Sticht H, Marx UC, Muller W, Rosch P, Schwarzinger S (2003) CD and NMR studies of prion protein (prp) helix 1—novel implications for its role in the $PrP^{C} \rightarrow PrP^{Sc}$ conversion process. J Biol Chem 278:50175–50181

Zuckerman DM, Lyman E (2006) A second look at canonical sampling of biomolecules using replica exchange simulation. J Chem Theory Comput 2:1200–1202